Edge tool influence function library using the parametric edge model for computer controlled optical surfacing

Dae Wook Kim*[a], Won Hyun Park[a], Sug-Whan Kim[b], and James H. Burge [a]
[a] College of Optical Sciences, Univ. of Arizona, 1630 E. University Blvd, Tucson, AZ 85721, USA;
[b] Space Optics Laboratory, Dept. of Astronomy, Yonsei Univ., 134 Sinchon-dong, Seodaemun-gu, Seoul 120-749, Republic of Korea

ABSTRACT

Computer controlled optical surfacing (CCOS) requires accurate knowledge of the tool influence function (TIF) for the polishing tool. The linear Preston's model for material removal has been used to determine the TIF for most cases. As the tool runs over the edge of the workpiece, however, nonlinear removal behavior needs to be considered to model the edge TIF. We reported a new parametric edge TIF model in a previous paper.** This model fits 5 parameters to measured data to accurately predict the edge TIF. We present material from the previous paper, and provide a library of the parametric edge TIFs for various tool shape and motion cases. The edge TIF library is a useful reference to design an edge figuring process using a CCOS technique.

Keywords: edge tool influence function, edge removal, Preston's model, edge TIF library

1. INTRODUCTION

Many Computer Controlled Optical Surfacing (CCOS) techniques have been presented and developed since 1972 [1-8]. The CCOS with its superb ability to control material removal is known as an ideal method to fabricate state-of-the-art optical surfaces, such as meter-class optics, segmented mirrors, off-axis mirrors, and so forth [5-7, 9].

The demand for an efficient workpiece edge figuring process using the CCOS techniques have been increased due to the popularity of segmented optics in many next generation optical systems, such as the Giant Magellan Telescope (GMT) [10] and James Webb Space Telescope (JWST) [11]. Since those systems have multiple mirror segments as their primary or secondary mirrors, i) the total length of edges is much larger than the conventional system with one mirror; ii) the edges are distributed across the whole pupil.

The dwell time map of a tool on the workpiece is usually the primary control parameter to achieve a target removal (i.e. form error on the workpiece) as it can be modulated via altering the transverse speed of the tool on the workpiece [1-8, 12]. In order to calculate an optimized dwell time map, the CCOS mainly relies on a de-convolution process of the target removal using a Tool Influence Function (TIF) (i.e. the material removal map for a given tool and workpiece motion). Thus, having an edge TIF library (i.e. collection of the edge TIFs) based on a realistic edge model is crucial for the edge figuring process using the CCOS techniques.

The TIF can be calculated based on the equation of material removal, Δz, which is known as the Preston's equation [9],

$$\Delta z(x,y) = \kappa \cdot P(x,y) \cdot V_T(x,y) \cdot \Delta t(x,y) \tag{1}$$

where Δz is the integrated material removal from the workpiece surface, κ the Preston coefficient (i.e. removal rate), P pressure on the tool-workpiece contact position, V_T magnitude of relative speed between the tool and workpiece surface and Δt dwell time. It assumes that the integrated material removal, Δz, depends on P, V_T and Δt linearly.

* letter2dwk@hotmail.com; phone: 1 520 626 0486

** Section 1 ~ 4 is mainly from the previous paper without change [16].

Optical Manufacturing and Testing VIII, edited by James H. Burge, Oliver W. Fähnle, Ray Williamson,
Proc. of SPIE Vol. 7426, 74260G · © 2009 SPIE · CCC code: 0277-786X/09/$18 · doi: 10.1117/12.828499

It is well known that a nominal TIF calculated by integrating Eq. (1) under a moving tool fits well to experimental (i.e. measured) TIF as long as the tool stays inside the workpiece [9]. However, once the tool overhangs the edge of workpiece, the measured TIF tends to deviate from the nominal behavior due to dramatically varying pressure range, tool bending, and non-linear effects due to tool material (e.g. pitch) flow [13].

Assuming the linearity of Preston's equation the edge effects can be associated with the pressure distribution on the tool-workpiece contact area. R. A. Jones suggested a linear pressure distribution model in 1986 [6]. Luna-Aguilar, et al.(2003) and Cordero-Davila, et al.(2004) developed this approach further using a non-linear high pressure distribution near the edge-side of the workpiece, however they did not report the model's validity by demonstrating it using experimental evidence [14, 15].

For any real polishing tool, the actual removal distribution is a complex function of many factors such as tool-workpiece configuration, tool stiffness, polishing compounds, polishing pad, and so forth. The analytical pressure distribution, *p(x,y)*, approaches [6, 14, 15] tend to ignore some of these effects. Also, in the edge TIF cases, the linearity for Preston's equation may need to be re-considered since the pressure distribution changes in wide pressure value range. The linearity is usually valid for a moderate range of pressure, *P*, values for a given polishing configuration [13].

Rather than assigning the edge effects to a certain type of analytical pressure distribution model, we define a parametric model based on measured data that allows us to create an accurate TIF without the need of identifying the actual cause of the abnormal behavior in edge removal. We then re-defined the Preston coefficient, κ, which has been regarded as a universal constant in the spatial domain as a function of position in the TIF via the parametric approach. By doing so, we can simulate the combined net effect of many complex factors without adding more terms to the original Preston's equation, Eq. (1).

This paper describes the parametric edge TIF model and provides an edge TIF library for various CCOS parameters, such as tool shape, size and motion. Section 2 deals with the theoretical background supporting the parametric edge TIF model. We introduce a functional form of the κ map, and show simulated parametric edge TIFs from the model in Section 3. The experimental demonstration and value of the parametric edge TIF model are summarized in Sections 4. The edge TIF library using the parametric edge model will be provided in Section 5 and Appendix A.

2. THEORETICAL BACKGROUND FOR THE PARAMETRIC EDGE TIF MODEL

2.1 Linear pressure distribution model

Assuming the linear pressure distribution and Preston's relation, we determine the resulting TIF analytically. Assume local coordinate system, (x, y), centered at the workpiece edge with the x axis in the overhang direction (i.e. the radial direction from the workpiece center). The pressure distribution under the tool-workpiece contact area should satisfy two conditions [15]. i) The total force, f_0, applied on the tool should be the same as the integral of the pressure distribution, *p(x,y)*, over the tool-workpiece contact area, A. ii) The total sum of the moment on the tool should be zero. It is assumed that the pressure distribution in y direction is constant, and it is symmetric with respect to the x axis. The moment needs to be calculated about the center of mass of the tool, (x', y') [15]. These two conditions are expressed in Eq. (2) and (3), respectively.

$$\iint_A p(x,y)dxdy = f_0 \tag{2}$$

$$\iint_A (x-x')\cdot p(x-x',y)dxdy = 0 \tag{3}$$

where x' is the x coordinate of the center of mass of the tool.

R.A. Jones introduced the linear pressure distribution model, Eq. (4), in 1986 [6] on the tool-workpiece contact area.

$$p(x,y) = c_1 \cdot x + c_2 \tag{4}$$

The pressure distribution, *p(x,y)*, is determined by solving two equations, Eq. (2) and (3), for two unknown coefficients, c_1 and c_2. Some examples of the linear pressure distribution, *p(x)*, are plotted in Fig. 1 (left) when a circular tool

overhang ratio, S_{tool}, changes from 0 to 0.3. S_{tool} is defined as the ratio of the overhang distance, H, to the tool width in the overhang direction, W_{tool}, in Fig. 1 (left).

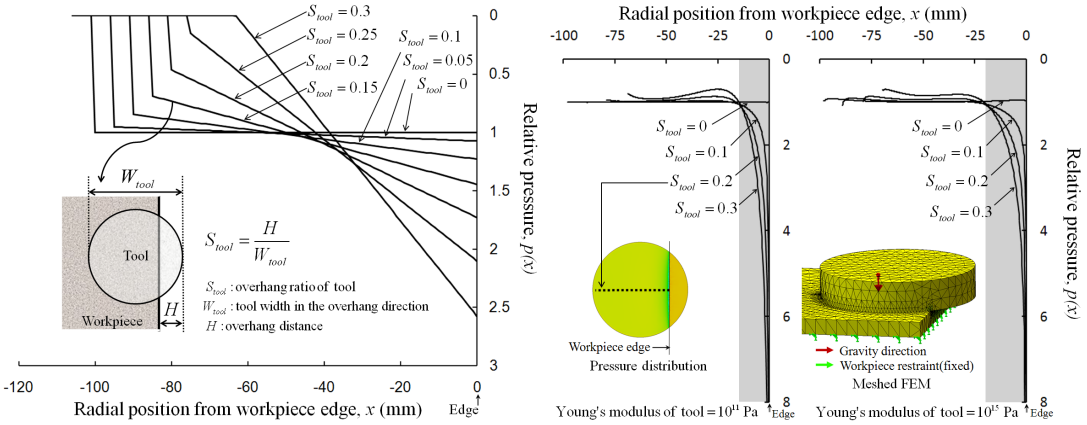

Fig. 1. x-profiles of the pressure distribution, $p(x,y)$, under the tool-workpiece contact area: linear pressure distribution model. (left), static FEA results. (right)

2.2 The first (edge-side) correction Section

One of the well-known edge removal anomalies is the 'turned-down edge', excessively high removal relative to the target removal near the edge-side [13]. This effect, as shown in the top-right quadrant of Fig. 7 later, cannot be explained by the linear pressure distribution model (i.e. basic edge TIF model).

Static Finite Element Analysis (FEA) was performed to characterize a general trend of the edge pressure distribution when tools with different stiffnesses overhang a workpiece. A circular tool and a workpiece were created in a solid model as shown in Fig. 1 (right). The Young's modulus of the tool was changed to simulate the effects of the tool stiffness. The tool was deformed by gravity, and the pressure distribution in the gravity direction was calculated under the tool-workpiece contact area.

Two of the FEA results are shown in Fig. 1 (right). There are two major trends in common for most of the FEA results. i) There is a non-linear high pressure distribution in the edge-side, shaded region in Fig. 1 (right). ii) The range of this non-linear distribution remains about same although the overhang ratio, S_{tool}, varies.

The first correction term, f_1, described in detail later in Section 3.2 is formed to correct this edge-side phenomenon.

2.3 The second (workpiece-center-side) correction

Experimentally it was found that the high pressure distribution model used on the edge-side of the tool did not predict the measured behavior at the other side (i.e. workpiece-center-side) of the tool. For an example, more removal than the predicted removal based on the basic edge TIF was observed in the workpiece-center-side of the experimental edge removal profile as shown in the top-right quadrant of Fig. 7. This phenomenon cannot be explained using models which focus only on the edge-side effects. Therefore, we define a second correction term, f_2, to address this discrepancy in Section 3.2.

3. PARAMETRIC EDGE TIF MODEL

3.1 Generation of the basic edge TIF

For a given tool motion and pressure distribution under the tool-workpiece contact area, a basic edge TIF can be calculated using Eq. (1) and the linear pressure model in Section 2.1 [9]. Two types of tool motion, orbital and spin, were used in this paper. i) Orbital: The tool orbits around the TIF center with orbital radius, $R_{orbital}$, and does not rotate. ii) Spin: The tool rotates about the center of the tool. These tool motions are depicted in Fig. 2.

The tool overhang ratio, S_{tool}, is fixed for the spin tool motion case, but varies as a function of tool position (A~F in Fig. 2 (left)) for the orbital case while the basic edge TIF calculation is being made.

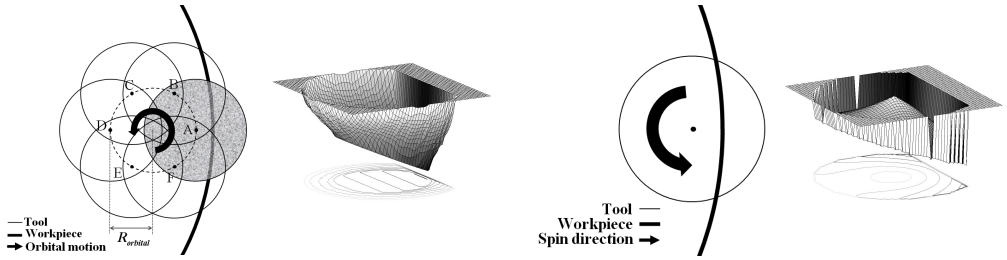

Fig. 2. Orbital (left) and spin (right) tool motion with the basic edge TIF.

3.2 Spatially varying Preston coefficient (κ) map

A new concept using the κ map for the parametric edge TIF model is introduced. The κ map represents the spatial distribution of the Preston coefficient, $\kappa(x,y)$, on the basic edge TIF that already includes the linear pressure gradient. It changes as a function of TIF overhang ratio, S_{TIF}, and five function control parameters (α, β, γ, δ and ε). S_{TIF} is defined as the ratio of the overhang distance, H, to the TIF width in the overhang direction, W_{TIF}, in Fig. 3. The parametric edge TIF can be calculated by multiplying the basic edge TIF by the κ map. The κ map is defined by a local coordinate centered at the edge of the workpiece. x represents the radial position from the workpiece edge.

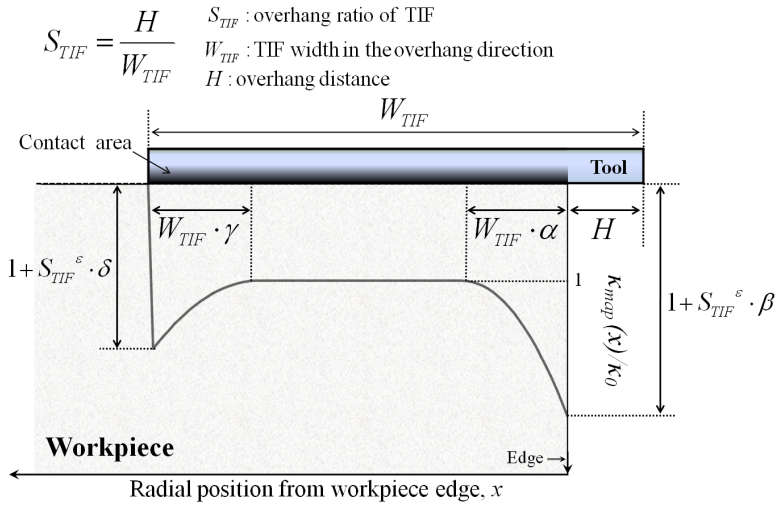

Fig. 3. Degrees of freedom of the κ map (in x-profile) using five parameters.

The edge-side high removal mentioned earlier in Section 2.2 is approximated by the first quadratic correction term, f_1, with two parameters, α and β. The first parameter, α, determines the range of the quadratic correction from the edge of the workpiece. The second parameter, β, controls the magnitude of the correction. This degree of freedom using α and β is shown in Fig. 3. This correction is shown graphically in Fig. 3 and defined analytically as

$$f_1(x,\alpha,\beta) = \frac{\beta}{(W_{TIF}\cdot\alpha)^2}\cdot(x + W_{TIF}\cdot\alpha)^2 \cdot \Theta(x + W_{TIF}\cdot\alpha) \tag{5}$$

where $\Theta(z)$ is the step function; 1 for $z \geq 0$ and 0 for $z < 0$.

The second correction term, f_2, to address the discrepancy between the simulated edge removal using basic edge TIF and measured edge removal in the workpiece-center-side region (mentioned in Section 2.3) is defined by Eq. (6). Similar to f_1, it has two parameters, γ and δ. The third parameter, γ, determines the range of the second correction, and the fourth parameter, δ, controls the magnitude of the correction as shown in Fig. 3.

$$f_2(x,\gamma,\delta) = \frac{\delta}{(W_{TIF}\cdot\gamma)^2}\cdot(-x - W_{TIF} + W_{TIF}\cdot S_{TIF} + W_{TIF}\cdot\gamma)^2 \cdot \Theta(-x - W_{TIF} + W_{TIF}\cdot S_{TIF} + W_{TIF}\cdot\gamma) \tag{6}$$

The κ map is defined in Eq. (7). It is a sum of the first and second correction terms, and includes a fifth parameter, ε. The fifth parameter, ε, was introduced to change the magnitude of the κ map as a function of TIF overhang ratio, S_{TIF}. Larger ε means that required correction magnitude increases faster as overhang ratio increases.

$$\kappa_{map}(x,\alpha,\beta,\gamma,\delta,\varepsilon) = \kappa_0 \cdot \{1 + S_{TIF}{}^{\varepsilon} \cdot (f_1 + f_2)\} \tag{7}$$

where the κ_0 is the Preston coefficient when there is no overhang.

The x-profiles of example κ maps are plotted in Fig. 4. An arbitrary parameter set (α=0.2, β=2, γ=0.2, δ=1 and ε=0.2) was used in the example.

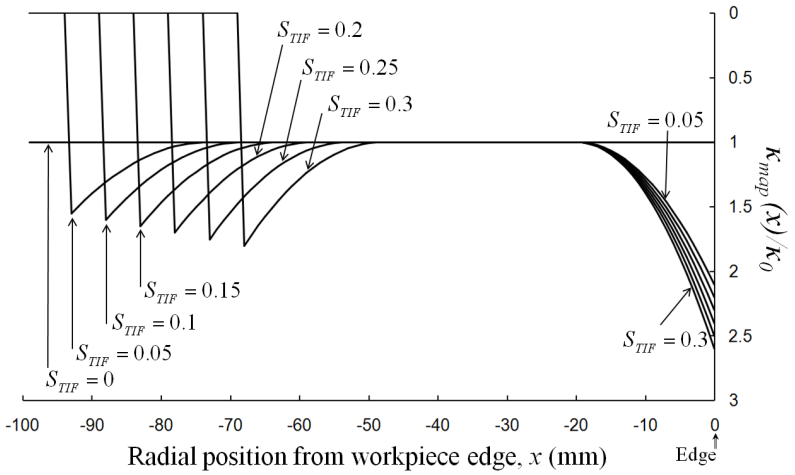

Fig. 4. x-Profiles of κ maps for various overhang ratio, S_{TIF}. (α=0.2, β=2, γ=0.2, δ=1 and ε=0.2).

3.3 Generation of the parametric edge TIF

The parametric edge TIFs for orbital and spin tool motion cases were generated by multiplying the κ map (i.e. the spatial distribution of the Preston's coefficient) by the basic edge TIF (with κ =1) introduced in Section 3.1. The overhang ratio, S_{TIF}, was varied from 0 to 0.3. Five parameter values (α, β, γ, δ, and ε) were used to fit the experimental data in Section 4.1 and 4.2. The parametric edge TIFs are shown in Table 1. As we increase the overhang ratio, S_{TIF}, non-linearly increasing removal near the workpiece edge is clearly shown as a result of the first correctional term for both the orbital and spin cases. The effects of the second correction are also observed. Due to the opposite signs of δ for the orbital (δ = 20) and spin (δ = -3) cases, in the workpiece-center-side region, there is more and less removal than the basic edge TIF's.

Table. 1. Normalized parametric edge TIFs

Tool motion	Overhang ratio, S_{TIF}				Scale
	0	0.1	0.2	0.3	
Orbital	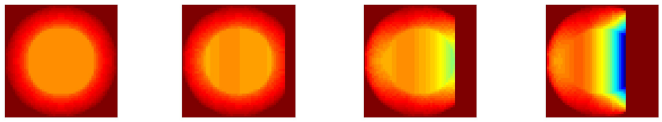				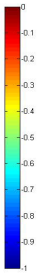
Spin	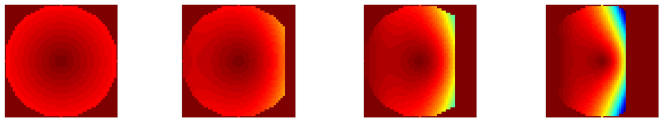				

(Orbital: α=0.2, β=4, γ=0.4, δ=20, ε=1.5 / Spin: α=0.4, β=6, γ=0.3, δ=-3, ε=0.9)

4. EXPERIMENTAL DEMONSTRATION OF THE PARAMETRIC EDGE TIF MODEL

Two sets of experiments were used to demonstrate the performance of the parametric edge TIF model. Because the workpiece was rotated in the experiments, integration of parametric edge TIF along the workpiece rotation direction was computed to get the integrated removal profile while considering the workpiece rotation velocity. These model based removal profiles are plotted in Fig. 5 and 6. The conditions for the two edge TIF experiments are provided in Table 2.

Table. 2. Edge TIF experiment conditions

Experiment Set No.		1	2
General	Run time	6 hours	1 hour
	Polishing compound	Hastlite ZD	Rhodite
Workpiece	Diameter	660mm	250mm
	Material	ULE	Pyrex
	Surface figure	Convex	Concave
	RPM	6	24
Tool	Polishing Material	Poly-Urethane pad	Poly-Urethane pad
	Diameter	172mm	100mm
	RPM	60 (orbital motion)	30 (spin motion)
	Tool motion	Orbital	Spin
	Orbital radius, $R_{orbital}$	20mm	N/A

4.1 Experimental set 1: Orbital tool motion

The first experimental set was performed using orbital tool motion on a ULE workpiece (w/ overhang ratio S_{TIF} = 0.05, 0.14, 0.24 and 0.28). The measured removal profiles with RMS error bars are plotted in Fig. 5. The simulated removal profiles based on the parametric edge TIF model (α=0.2, β=4, γ=0.4, δ=20 and ε=1.5) are also plotted. The five parameters were optimized to fit the experimental data. With one set of parameters, most of the simulated removal profiles for all overhang ratio cases are well fit to the measured removals within the RMS error bars.

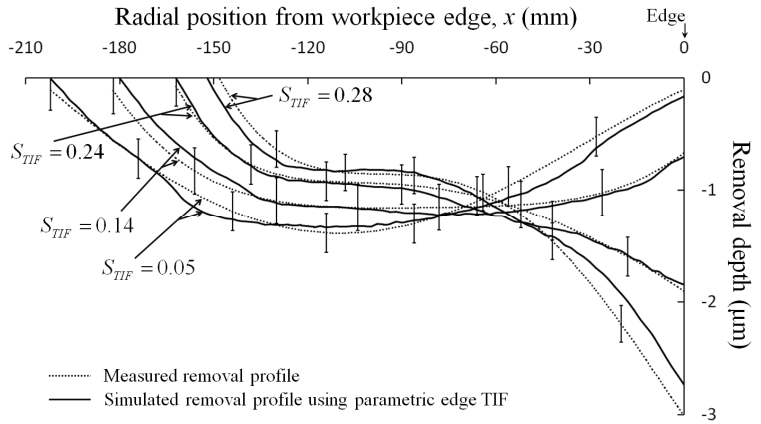

Fig. 5. Measured vs simulated removal profiles: orbital tool motion (α=0.2, β=4, γ=0.4, δ=20, and ε=1.5).

4.2 Experimental set 2: Spin tool motion

The second experimental set was performed using spin tool motion on a Pyrex workpiece. The overhang ratio, S_{TIF}, was changed to 0.02, 0.17, 0.22 and 0.4. The measured removal profiles with RMS error bars are plotted in Fig. 6. The simulated removal profiles based on the parametric edge TIF model are plotted also. They are reasonably well matched with the measured removal profiles for all overhang ratio cases including very high overhang ratio case, S_{TIF} = 0.4.

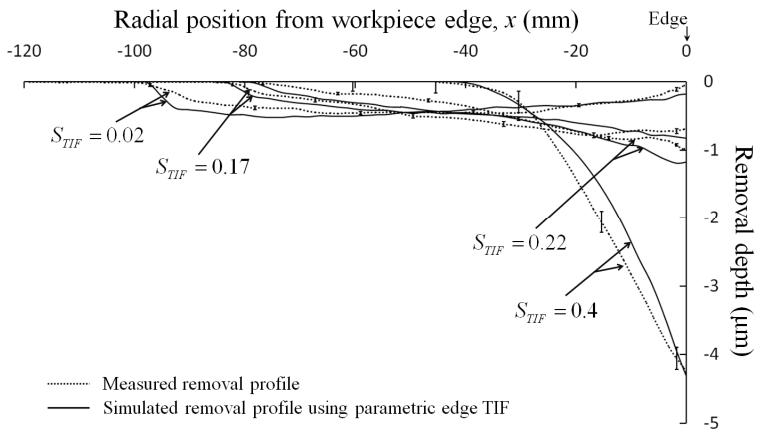

Fig. 6. Measured vs simulated removal profiles: spin tool motion case (α=0.4, β=6, γ=0.3, δ=-3, and ε=0.9).

4.3 Performance of the parametric edge TIF model

The comparison between the four different edge TIF models is shown in Fig. 7. The simulated removal profile based on nominal (i.e. no edge model) TIF model does not follow the overall slope of the measured removal profile. Especially, it shows a large difference in the edge-side removal (x = 0 ~ -60mm). The computed removal profile using basic edge TIF model seems to have a closer overall slope to the measured removal. However, two mismatches between the measured and simulated removal are clearly observed in the edge-side and workpiece-center-side regions. The parametric edge TIF model using only the first correction allows us to correct the discrepancy in the edge-side removal. The removal profile based on the parametric edge TIF model using both the first and second correction is well matched with the experimental removal profile over the whole range of the removal profile.

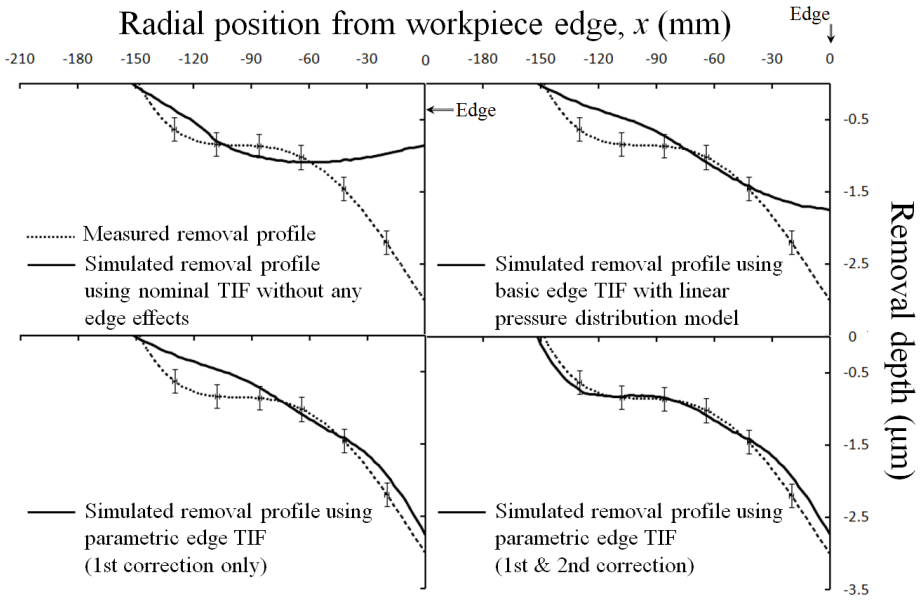

Fig. 7. Measured (with RMS error bars) vs simulated (using different edge TIF models) edge removal profiles for the orbital tool motion case.

The comparison between the four TIF models is presented in Fig. 8. We define normalized fit residual, Δ, as a figure of merit to quantify the performance of the parametric model compared to the data. This is normalized as

$$\Delta = normalized\ fit\ residual = \frac{RMS\ of\ (data - model)}{RMS\ of\ data} \cdot 100\ (\%) \tag{8}$$

It is clear that the normalized fit residual, Δ, is relatively low (about 10~20%) for all TIF model cases when the overhang ratio is small (S_{TIF} <0.14 for orbital case and S_{TIF} <0.02 for spin case). It basically means that there is no difference between nominal and edge TIF models when the overhang effects are negligible.

The improvements become significant as the overhang ratio increases. For the orbital tool motion case with S_{TIF}=0.28, the normalized fit residual, Δ, falls to 10% (parametric edge TIF using both corrections) from 52% (nominal TIF), or from 30% (basic edge TIF). For the spin tool motion case with S_{TIF}=0.4, the normalized fit residual, Δ, is dramatically improved to 12% (parametric edge TIF using both corrections) from 87% (nominal TIF), or from 66% (basic edge TIF).

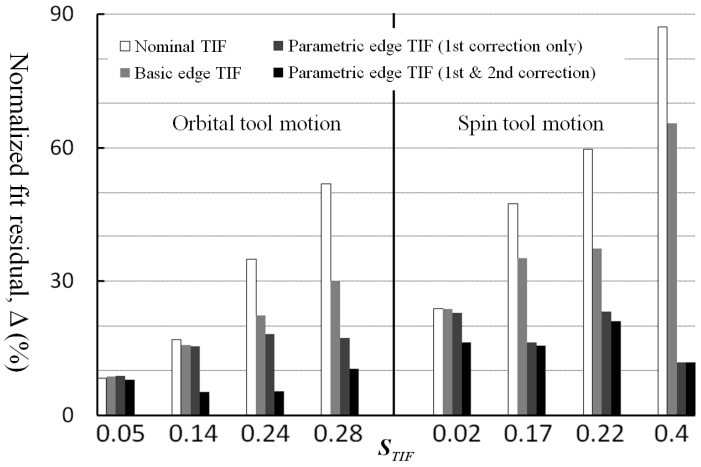

Fig. 8. Normalized fit residual, Δ, of the simulated removal profiles using different TIF models for orbital and spin tool motions.

5. PARAMETRIC EDGE TIF LIBRARY

5.1 Generation of the TIF library

A TIF is the material removal map for a given specific CCOS configuration, which includes tool shape, tool motion, workpiece motion, tool position and so forth. For instance, the TIF is a function of the tool position on the workpiece since the relative motion between the tool and workpiece changes as the tool moves on the workpiece.

The TIF library is a collection of these TIFs at various positions on the workpiece for a given polishing configuration. The shape, size and magnitude of the TIFs are directly related with the tool size, tool motion, and tool shape.

5.2 Parametric edge TIF library

The parametric edge TIF library was generated from the edge model for various tool shapes, tool motions, and tool sizes. We assumed same control parameter values as the experimental cases in Section 4.1 and 4.2 (Orbital tool motion: α=0.2, β=4, γ=0.4, δ=20, ε=1.5 and Spin tool motion: α=0.4, β=6, γ=0.3, δ=-3, ε=0.9). The relative rotation speed between the tool and workpiece was also varied since it plays an important role to determine the TIF shapes. These CCOS configuration parameters for the TIF library are listed in Appendix A.1. The parametric edge TIF library is provided in Appendix A.2.

The tool shape and its edge TIF (S_{TIF} = 0.3) are presented in the second and third column of the library table in Appendix A.2. The edge TIF is the material removal map under the tool-workpiece contact area when the tool overhangs. The ring TIF is the removal map when the workpiece rotates under the tool motion. This removal map looks like a ring (e.g. donut) on the workpiece. The relative speed between the tool motion and the workpiece rotation was considered to generate it. This is a function of the radial position of the edge TIF center, ρ, on the workpiece. The ring TIF profiles in Appendix A.2 only displays for ρ = 75, 80, 85, 90cm (i.e. S_{TIF} = 0, 0.1, 0.2, 0.3) cases in this paper. The full TIF library includes the ring TIFs for all ρ values.

Different tool shapes (circle, ellipse, square, and so forth) with different tool motions (spin and orbital) were used to generate the TIF library No.1 ~ 10. The relative speed between the tool and workpiece motion was changed in TIF library No. 11 ~ 20.

6. CONCLUDING REMARKS

We presented a parametric edge TIF library based on the parametric edge model that allows accurate simulation of edge effects when a tool overhangs the workpiece edge. This parametric edge TIF library is used to design (or optimize) an edge figuring process using the CCOS techniques [17]. Unlike other approaches using analytical pressure distributions to develop edge TIF models, we introduced a parametric approach using a κ map, which represents the spatial distribution of the Preston coefficient. In this way, we were able to express the net effects of many entangled factors affecting the edge removal process in terms of a parametric κ map.

Experimental verification was successfully performed. The normalized fit residual, Δ, for the simulated removal using the parametric edge TIF model stayed in the 5~20% range for all overhang cases, which allows us to correct about 80% of the surface errors (with an assumption that everything else is ideal) in a single CCOS process using the parametric edge TIF library. It means that more than 99% of the initial surface errors can be corrected in 3 CCOS runs. Improvement in convergence rate for the residual surface form error is directly related to more efficient time management and lower cost for large optics fabrication projects. Its significance would be even greater for segmented optical system projects, such as GMT [10] and JWST [11], which have more edges across the whole pupil.

APPENDIX A. PARAMETRIC EDGE TIF LIBRARY

A.1 Parameters for the parametric edge TIF library

Library ID #	Tool RPM	Workpiece RPM	Tool width (cm)	Tool motion	Orbital radius, $R_{orbital}$ (cm)	Tool shape
1	60	0.01	50	Spin	N/A	Circle
2	60	0.01	50	Spin	N/A	Donut
3	60	0.01	40	Orbital	5	Circle
4	60	0.01	40	Orbital	5	Donut
5	60	0.01	40	Orbital	5	Donut
6	60	0.01	40	Orbital	5	Ellipse
7	60	0.01	40	Orbital	5	Ellipse
8	60	0.01	40	Orbital	5	Square
9	60	0.01	40	Orbital	5	Rectangle
10	60	0.01	40	Orbital	5	Rectangle
11	60	-15	50	Spin	N/A	Circle
12	60	-5	50	Spin	N/A	Circle
13	60	1	50	Spin	N/A	Circle
14	60	5	50	Spin	N/A	Circle
15	60	15	50	Spin	N/A	Circle
16	60	-3	40	Orbital	5	Circle
17	60	-1	40	Orbital	5	Circle
18	60	0.01	40	Orbital	5	Circle
19	60	1	40	Orbital	5	Circle
20	60	3	40	Orbital	5	Circle

i) Preston constant [8] was assumed as -100 um/psi(m/sec)hour with 1 PSI tool pressure.
ii) Positive and negative RPM means clockwise and counterclockwise rotation, respectively.
iii) Tool width is measured in the overhang direction.
iv) Workpiece radius was assumed as 100cm.

A.2 Parametric edge TIF library

ID #	Tool Shape (cm × cm)	Normalized edge TIF (cm × cm)	Ring TIF radial, *r*, profiles on the workpiece (*r* axis in cm)
1	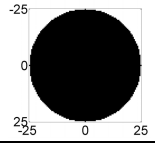	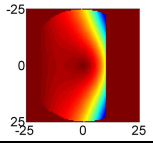	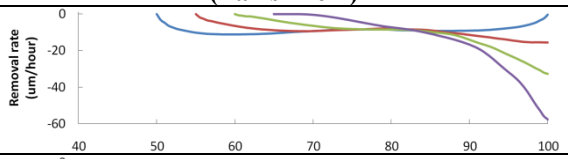
2	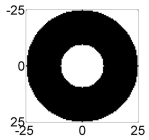	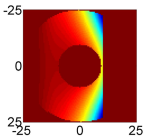	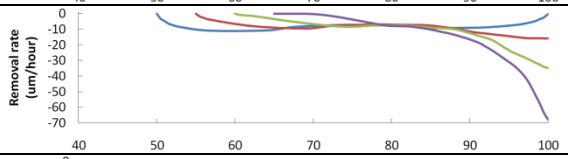
3	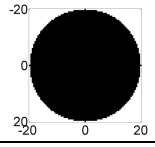	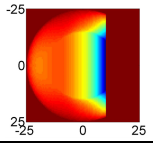	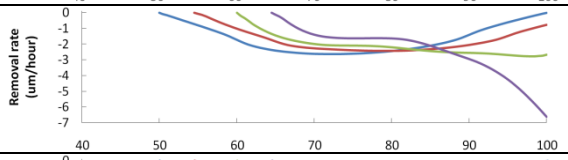
4	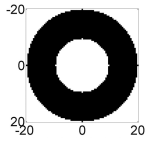	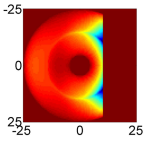	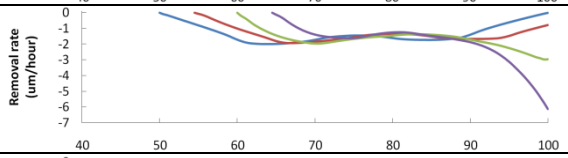
5	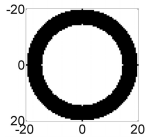	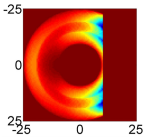	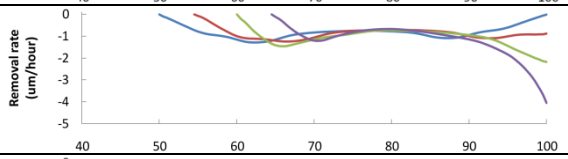
6	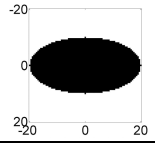	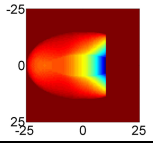	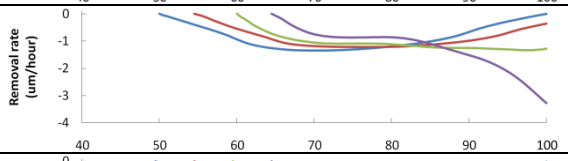
7	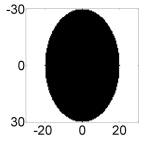	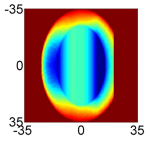	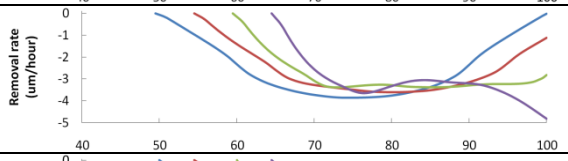
8	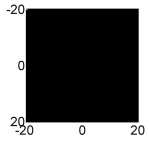	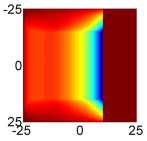	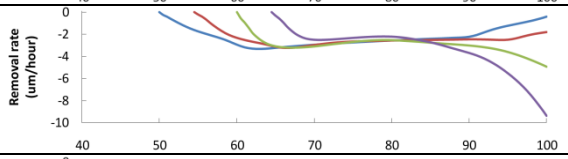
9	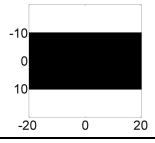	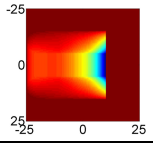	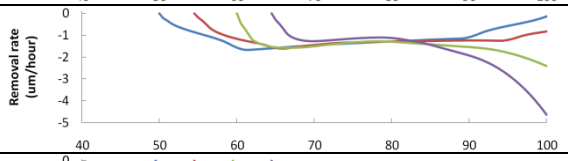
10	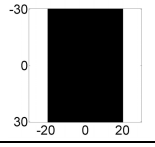	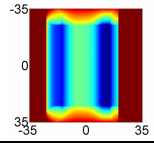	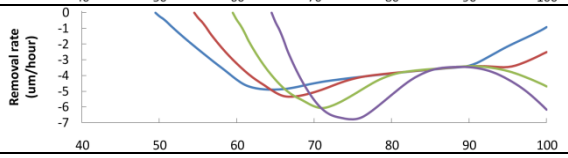

ID #	Tool Shape (cm × cm)	Normalized edge TIF (cm × cm)	Ring TIF radial, *r*, profiles on the workpiece (*r* axis in cm)
11	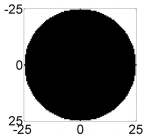	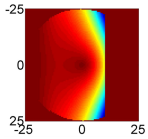	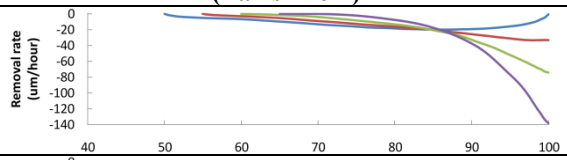
12	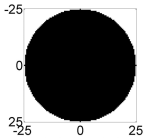	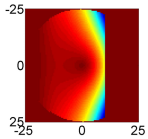	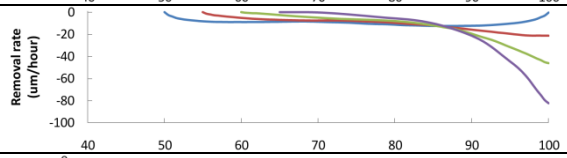
13	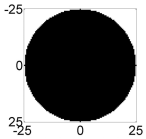	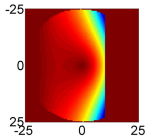	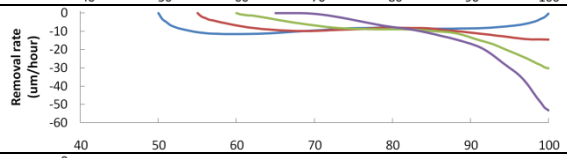
14	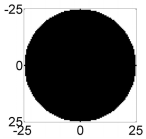	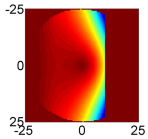	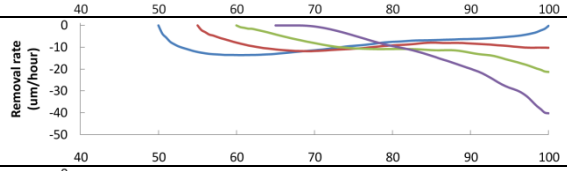
15	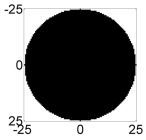	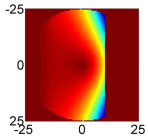	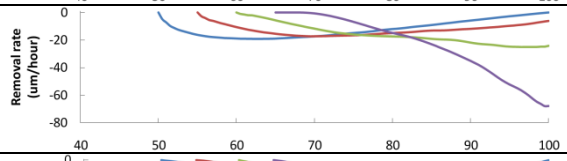
16	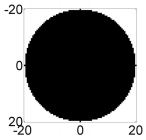	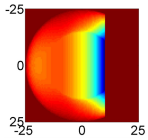	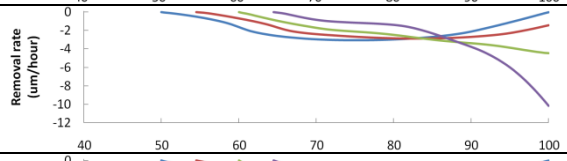
17	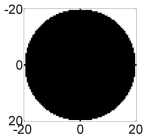	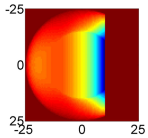	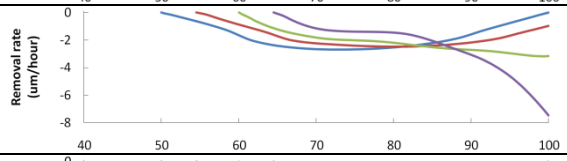
18	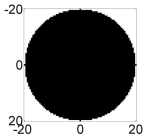	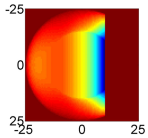	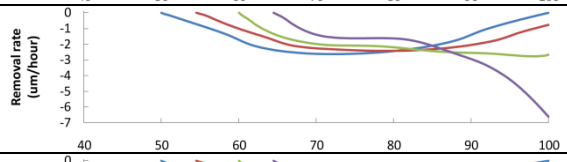
19	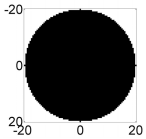	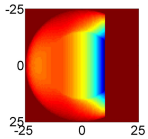	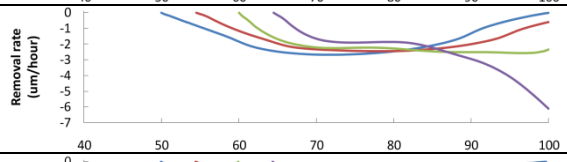
20	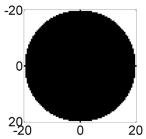	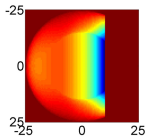	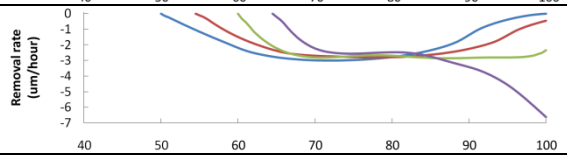

i) Overhang ratio for the ring TIF profiles: S_{TIF} = 0 (blue), 0.1 (red), 0.2 (green), 0.3 (purple)
ii) Edge model parameters for the orbital tool motion: α=0.2, β=4, γ=0.4, δ=20, ε=1.5
iii) Edge model parameters for the spin tool motion: α=0.4, β=6, γ=0.3, δ=-3, ε=0.9
iv) Normalized edge TIF uses same color scale as the edge TIF in Table. 1.

ACKNOWLEDGMENTS

We acknowledge that this work was supported by the Optical Engineering and Fabrication Facility of the College of Optical Sciences at the University of Arizona. We thank Buddy Martin (Steward Observatory Mirror Lab), Anoopoma Bhowmik, and Robert Parks (College of Optical Sciences) at the Univ. of Arizona for assistance in the final manuscript preparation.

REFERENCES

[1] R. Aspden, R. McDonough, and F.R. Nitchie, Jr, "Computer assisted optical surfacing," Appl. Opt. **11**, 2739-2747 (1972).

[2] R. E. Wagner and R. R. Shannon, "Fabrication of aspherics using a mathematical model for material removal," Appl. Opt. **13**, 1683-1689 (1974).

[3] D.J. Bajuk, "Computer controlled generation of rotationally symmetric aspheric surfaces," Opt. Eng. **15**, 401-406 (1976).

[4] R.A. Jones, "Grinding and polishing with small tools under computer control," Opt. Eng. **18**, 390-393 (1979).

[5] R.A. Jones, "Computer-controlled polishing of telescope mirror segments," Opt. Eng. **22**, 236-240 (1983).

[6] R.A. Jones, "Computer-controlled optical surfacing with orbital tool motion," Opt. Eng. **25**, 785-790 (1986).

[7] J.R. Johnson and E. Waluschka, "Optical fabrication-process modeling-analysis tool box," Proc. SPIE **1333**, 106-117 (1990).

[8] R.A. Jones and W.J. Rupp, "Rapid optical fabrication with CCOS," Proc. SPIE **1333**, 34-43 (1990).

[9] D.W. Kim and S.W. Kim, "Static tool influence function for fabrication simulation of hexagonal mirror segments for extremely large telescopes," Opt. Express. **13**, 910-917 (2005).

[10] Matt Johns, "The Giant Magellan Telescope (GMT)," Proc. SPIE **6986**, 698603 (2008).

[11] Mark Clampin, "Status of the James Webb Space Telescope (JWST)," Proc. SPIE **7010**, 70100L (2008).

[12] D.D. Walker, A.T. Beaucamp, D. Brooks, V. Doubrovski, M. Cassie, C. Dunn, R. Freeman, A. King, M. Libert, G. McCavana, R. Morton, D. Riley, and J. Simms, "New results from the Precessions polishing process scaled to larger sizes," Proc. SPIE **5494**, 71-80 (2004).

[13] Bob C. Crawford, Don Loomis, Norm Schenck, and Bill Anderson, Optical Engineering and Fabrication Facility, University of Arizona, 1630 E. University Blvd, Tucson, Arizona 85721, (personal communication, 2008).

[14] Luna-Aguilar E., Cordero-Davila A., Gonzalez Garcia J., Nunez-Alfonso M., Cabrera-Pelaez V.H., Robledo-Sanchez C., Cuautle-Cortez J., and Pedrayes-Lopez M. H., "Edge effects with Preston equation," Proc. SPIE **4840**, 598-603 (2003).

[15] Alberto Cordero-Davila, Jorge Gonzalez-Garcia, Maria Pedrayes-Lopez, Luis Alberto Aguilar-Chiu, Jorge Cuautle-Cortes, and Carlos Robledo-Sanchez, "Edge effects with the Preston equation for a circular tool and workpiece," Appl. Opt. **43**, 1250-1254 (2004).

[16] D.W. Kim, W.H. Park, S.W. Kim and J.H. Burge, " Parametric modeling of edge effects for polishing tool influence functions," Opt. Express. **17**, 5656-5665 (2009).

[17] Dae Wook Kim, College of Optical Sciences, University of Arizona, 1630 E. University Blvd, Tucson, Arizona 85721, S.W. Kim, and James H. Burge are preparing a manuscript to be called "Computer controlled optical surfacing technique using multiple TIF libraries."